

Tracking Autoionizing-Wave-Packet Dynamics at the 1-fs Temporal Scale

E. Skantzakis,¹ P. Tzallas,^{1,*} J. E. Kruse,¹ C. Kalpouzos,¹ O. Faucher,² G. D. Tsakiris,³ and D. Charalambidis^{1,4}

¹*Foundation for Research and Technology—Hellas, Institute of Electronic Structure and Laser,
P.O. Box 1527, GR-711 10 Heraklion, Crete, Greece*

²*Laboratoire Interdisciplinaire Carnot de Bourgogne, CNRS, Université de Bourgogne, UMR 5209,
9 Avenue Alain Savary, BP 47 870, F-21078 Dijon Cedex, France*

³*Max-Planck-Institut für Quantenoptik, Hans-Kopfermann-Straße 1, D-85748 Garching, Germany*

⁴*Department of Physics, University of Crete, P.O. Box 2208, GR71003 Heraklion, Crete, Greece*

(Received 19 March 2010; published 22 July 2010)

We present time-resolved studies and Fourier transform spectroscopy of inner-shell excited states undergoing Auger decay and doubly excited autoionizing states, utilizing coherent extreme-ultraviolet (XUV) radiation continua. Series of states spanning a range of ~ 4 eV are excited simultaneously. An XUV probe pulse tracks the oscillatory and decaying evolution of the formed wave packet. The Fourier transform of the measured trace reproduces the spectrum of the series. The present work paves the way for ultrabroadband XUV spectroscopy and studies of ultrafast dynamics in all states of matter.

DOI: 10.1103/PhysRevLett.105.043902

PACS numbers: 42.65.Re, 32.80.Ee, 32.80.Zb, 42.65.Ky

Linear interferometry is equivalent to frequency domain spectroscopy, as postulated in the Wiener-Khinchin theorem [1]. Time domain spectroscopic techniques such as optical Ramsey spectroscopy [2] or Fourier transform spectroscopy (FTS) are based on this principle. Optical pulses can essentially excite a single electronic state or a few very close lying electronic states. Broadband extreme-ultraviolet (XUV) radiation may significantly increase temporal resolution and excite coherent superpositions of state manifolds spanning a large part of an electronic spectrum. Along this perspective, the present work demonstrates the tracking of 1 fs-scale electron dynamics of a spectrally ultrabroad electronic wave packet.

The temporal evolution of a coherently excited superposition $|\psi\rangle$ of an atomic ground state $|g\rangle$, and a number (N) of energetically nondegenerate decaying eigenstates $|i\rangle$ and continuum states $|c\rangle$,

$$|\psi(t)\rangle = |g\rangle + \sum_i^N n_i(t) e^{-i(\omega_i t + \varphi_i)} e^{-\Gamma_i t} |i\rangle + \int dE c_n c(t) |c\rangle \quad (1)$$

[where $n_i(t)$ is the time-dependent probability amplitude of each excited state $|i\rangle$ with energy $E_i = \hbar\omega_i$, φ_i its initial phase, and Γ_i the decay rate of the state], features a multi-exponential decay superimposed by fast oscillations at frequencies ω_i that beat at frequencies $\omega_i - \omega_j = \Delta E_{ij}/\hbar$ (with $i, j = 1, \dots, N$). Such dynamics undergo, e.g., a superposition of autoionizing states (AIS). When the spacing ΔE_{ij} of the states is of the order of 10 meV, the beating period is “long,” of the order of 100 fs, and thus fs pulses are sufficient for probing the dynamics [3]. For ΔE_{ij} values of a few eV the beating period becomes 1 fs or shorter, the probing of which requires attosecond pulses [4]. Coherent broadband continuum XUV radiation, sup-

porting sub-fs pulse durations, like the radiation produced by the recently developed interferometric polarization gating (IPG) technique [5], at sufficiently high pulse energies [6], is an ideal tool for such studies. The tracking of the dynamics of the excited manifold may be accurately implemented utilizing two time-delayed pulse replicas produced by a split mirror autocorrelator [7–10]. The first pulse excites an electronic wave packet like the one of Eq. (1), thus inducing an atomic dipole that oscillates at the frequencies ω_i . The second pulse induces a phase shifted dipole, the phase shift being determined by the variable delay $\Delta\tau$ between the two pulses. Alternating constructive and destructive interference between the two dipoles results in Ramsey fringing appearing in the autoionization signal measured as a function of $\Delta\tau$. Even when this high frequency fringing cannot be resolved, its beating at different $\omega_i - \omega_j$ frequencies can be observable in the interferogram of the ion signal. The contrast in the beating fringes is modulated with the delay, because of the different beating frequencies present. At the same time, it undergoes an exponential decay, due to the decay of the interfering amplitudes as a result of autoionization dissipation. Starting from Eq. (1) and following the derivation of previous works [11], one finds that the measured ionization signal reads $S(\Delta\tau) \propto \sum_{ij} e^{-(\Gamma_i + \Gamma_j)\Delta\tau} \cos[(\omega_i - \omega_j)\Delta\tau]$. Fano-Beutler parameters [12] are further incorporated as phase shifts in the interferometric trace. The Fourier transform of the measured trace gives the frequency spectrum of the manifold.

In the present work, the above method is applied to a manifold of inner-shell and doubly excited AIS of xenon [13–18] using coherent broadband continua spanning from 15 to 25 eV (FWHM). More precisely, the absorbed radiation excites a large part of the spectrum of the odd-parity Rydberg autoionizing series that includes doubly excited

$5s^25p^4[{}^3P, {}^1D, {}^1S]mlm'l'$ [15] states and $5s$ inner-shell excited $5s5p^6({}^2S_{1/2})np[{}^1P_1]$ states (with $6 \leq n \leq 12$) undergoing Auger decay. Figure 1 depicts the excitation scheme. The spectrum of this region is known from photoabsorption studies [14,17]. The energy differences between these states range from 4 meV to 2.4 eV. As the maximum delay $\Delta\tau_{\max}$ in this experiment was 220 fs, the frequency resolution was limited to 4.5 ps^{-1} so that peaks with separation smaller than $\sim 50 \text{ meV}$ could not be resolved.

The experiment has been performed utilizing a 10 Hz repetition rate Ti:Sapphire laser system delivering pulses of 80 mJ/pulse energy and $\tau_L = 40 \text{ fs}$ duration at a carrier wavelength of 800 nm. The XUV broadband coherent continuum radiation is generated by an IPG device [5,6]. The experimental setup, which is shown in Fig. 2(a), is described in detail elsewhere [6]. The generation occurs in a Xe gas jet, and the XUV radiation is reflected by a Si plate, placed at the Brewster's angle of 75° of the fundamental laser frequency. After reflection the XUV beam passes through a 3 mm diameter aperture and a 150 nm thick Sn filter in order to select the central part of the radiation with a central wavelength of $\sim 60 \text{ nm}$. The spectral intensity distribution of the XUV radiation was determined by measuring the energy-resolved, single-photon ionization, photoelectron spectra of Ar gas. The electrons produced by the interaction of the Ar gas with the XUV beam were detected by a μ -metal shielded time-of-flight (TOF) spectrometer. The spectrum of the radiation used in the experiment is shown in Fig. 2(b). This radiation can support isolated pulses with a duration as short as $\sim 450 \text{ as}$. The duration of the pulse has not been measured, as the available intensity was not sufficient for a second-order intensity volume autocorrelation [8]. The XUV beam was subsequently focused by a wave-front divider (split spherical gold mirror) of 5 cm focal length into a Xe pulsed gas jet. One half of the mirror is mounted on a feedback-controlled piezo-crystal translation stage with minimum

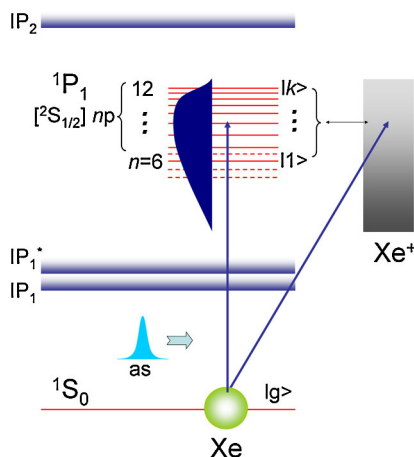


FIG. 1 (color online). Single-photon ionization scheme of Xe induced by a coherent broadband XUV radiation continuum.

longitudinal displacement of 1.5 nm. The xenon ions were recorded by the TOF ion mass spectrometer as a function of the delay $\Delta\tau$ between the two XUV replicas produced by the split mirror. It should be stressed that the ionization process in this work is not a two-XUV-photon process [19], in contrast to recent second-order intensity volume autocorrelation measurements [8]. It is a single-photon ionization and thus a first-order process, for which the split mirror wave-front divider is not an appropriate device [8], since, in principle, it operates only as a non-linear autocorrelator. The reason that a first-order process produces an observable beating trace here is that the measured signal does not originate from the entire interaction volume. The experimental setup (gas jet dimensions and focusing conditions) introduces a confinement of the interaction volume along the propagation axis. Moreover, the data of the trace are values of specific times of flight (line outs) of the mass spectra and not integrals of the entire ion mass peak, which introduces a partial confinement in a second dimension (along the TOF axis) as the TOF was not operated as to have a temporal focus. Because of this volume confinement the signal beating is not entirely vanishing through the spatial integration. This has been verified by first-order autocorrelation measurements (no excited states involved) and confirmed through modeling using the model reported in [10]. Measurements have been performed in two types of scans, a coarse scan with a delay step $\Delta\tau = 1.33 \text{ fs}$ addressing low frequency components (autoionizing state pairs with small energy differences) and a fine scan with a delay step $\Delta\tau = 0.333 \text{ fs}$ addressing high frequency components (autoionizing state pairs with large energy differences) of the spectrum. In both scans 100 data points were accumulated for each delay step.

Figure 3 shows traces of a coarse [grey dashed line in Fig. 3(a)] and a fine scan [grey dashed line in Fig. 3(c)]. The clearly observable interference fringes are the signature of the excited state superposition and reflect the temporal evolution of the formed wave packet. Figures 3(b) and 3(d) show the frequency spectrum (grey dotted lines)

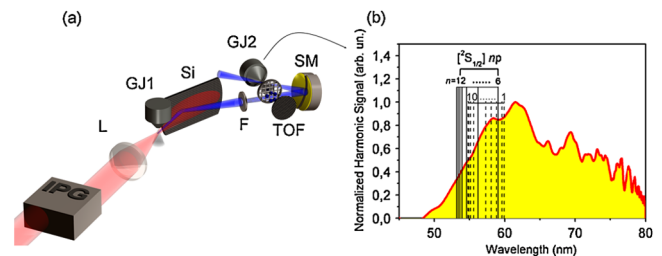


FIG. 2 (color online). (a) Experimental apparatus. IPG, interferometric polarization gating device; L, lens; GJ1, pulsed Xe gas jet; Si, silicon plate; F, Sn filter; GJ2, pulsed gas jet; TOF, time-of-flight spectrometer; SM, split mirror. (b) Spectrum of the coherent continuum XUV radiation. The black solid and dashed lines in (b) show the spectral position of the autoionizing states within the XUV radiation spectrum.

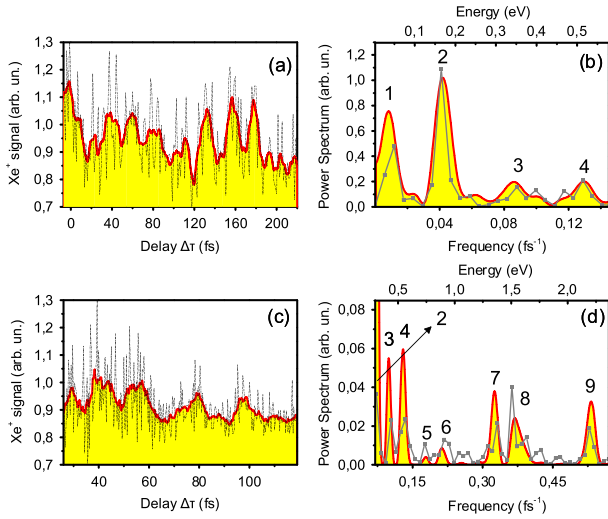


FIG. 3 (color online). Ultrafast autoionization dynamics measurement. (a) The trace shown by the grey dashed line is the autoionization signal as a function of the delay between the two XUV pulses, in a coarse scan. A higher-order autocorrelation trace of the fundamental laser field has been used for the calibration of the zero delay value ($\Delta\tau = 0 \pm 3$ fs) of the trace. (b) Frequency spectrum obtained from the Fourier transform of the raw data of the trace shown in (a). The numbering of the peaks refers to the autoionization states in Table I. (c) Traces as in (a) in a fine scan. (d) Frequency spectrum obtained from the Fourier transform of the raw data of the trace shown in (c).

resulting from the Fourier transform of the raw data for the coarse and fine scans, respectively, and the yellow-filled area below the red line shows the spectrum resulting from an interpolated discrete time Fourier transform (IDTFT) procedure [20] on the raw data. The peak frequencies are the excitation frequency differences of the autoionizing states. In Fig. 3(d) the first part of the spectrum, where

peak 2 appears with a large height, is not shown in order for the rest of the peaks to become better visible. Because of the stated limited energy resolution defined by the maximum delay available, not all states can be resolved. Each peak of Figs. 3(b) and 3(d) originates from the decay of more than one state. The states contributing to each peak are summarized in Table I. The configurations and numbers in parentheses give the pair of states contributing to each of the recorded frequency components. Configurations are given for the inner-shell excited states, while numbers represent doubly excited states $mlm'l'$ as described in the caption of Table I. Lifetimes of the states are given at the foot of the table. In order to enhance the visibility of the low frequency beating (<0.05 fs $^{-1}$), the moving averages of the raw data in the coarse and fine scans are taken over 7 and 20 points, respectively, and are shown in the yellow-filled areas under the red lines in Figs. 3(a) and 3(c).

To calculate the fringe contrast, we have used the ionization probability of Xe as obtained from the theoretical model of Ref. [11]. In the calculation, the widths Γ of the states, the Fano-Beutler parameters q , and the relative ionization cross sections σ are taken from Refs. [14,15]. The values of σ for the inner-shell excited autoionizing Rydberg states and the values of q for the states with energy in the region 22.5 eV $< E < 22.7$ eV have been extracted from Ref. [13]. The widths Γ of Rydberg states np with $9 \leq n \leq 12$ have been obtained through an extrapolation of the Γ data in the literature using $\Gamma(n) \propto 1/(n - \delta)^3$ as a fit function. The parameter δ is the quantum defect, which in the present extrapolation is found to be $\delta = 3.06$. It has been found that the states with energies higher than 23.2 eV have minor contributions to the general behavior of the calculated trace. The yellow-filled area below the blue (dark grey) line in Fig. 4 shows the calculated fringe contrast together with the contrast extracted

TABLE I. AIS contributing to the spectral distribution of Figs. 3(b) and 3(d). The numbers in the first column correspond to the numbering in Figs. 3(b) and 3(d). The second column gives the central frequencies ν of the peaks in Figs. 3(b) and 3(d). The third column shows the combination of the pairs of AIS contributing to each peak. States 1–10 are doubly excited states with energies (in eV) of 20.664, 20.805, 21.03, 21.407, 21.721, 22.333, 22.457, 22.514, 22.56, and 22.617, respectively. The lifetimes (in fs) of the 1–10 doubly excited and $[^2S_{1/2}]6p - [^2S_{1/2}]12p$ Rydberg states are 177, 80, 45, 113, 91, 100, 82, 110, 134, 94 and 21, 50, 105, 156, 276, 414, 590, respectively.

Peak no.	$\nu(10^{-3} \text{ fs}^{-1})$	Autoionization state pairs
1	9 ± 6	$([^2S_{1/2}]12p, [^2S_{1/2}]11p), ([^2S_{1/2}]8p, 7), (9, 8), (10, 9)$
2	42 ± 10	$([^2S_{1/2}]11p, [^2S_{1/2}]9p), ([^2S_{1/2}]6p, 2), ([^2S_{1/2}]8p, 8-9), (10,7), (6, 8), (2, 1)$
3	93 ± 10	$([^2S_{1/2}]11p - [^2S_{1/2}]10p, 8p), ([^2S_{1/2}]7p, 10), ([^2S_{1/2}]8p, 6), ([^2S_{1/2}]9p, 8-9), (4, 3)$
4	128 ± 10	$([^2S_{1/2}]12p, [^2S_{1/2}]8p), ([^2S_{1/2}]7p, 5), ([^2S_{1/2}]10p, 8-9)$
5	179 ± 10	$([^2S_{1/2}]9p, [^2S_{1/2}]7p), ([^2S_{1/2}]6p, 5), ([^2S_{1/2}]10p, 6), ([^2S_{1/2}]11p, 7),$ $([^2S_{1/2}]11p, 9-10), ([^2S_{1/2}]12p, 7-8), (7, 5), (4, 1)$
6	214 ± 15	$([^2S_{1/2}]7p, [^2S_{1/2}]11p - [^2S_{1/2}]10p), ([^2S_{1/2}]12p, 6), (5, 2), (4, 5-6), (5, 10)$
7	325 ± 15	$([^2S_{1/2}]6p, [^2S_{1/2}]7p), ([^2S_{1/2}]6p, 6), ([^2S_{1/2}]8p, 4), ([^2S_{1/2}]10p, 5), (6, 3)$
8	371 ± 20	$([^2S_{1/2}]6p, 7-10), ([^2S_{1/2}]7p, 1), ([^2S_{1/2}]9p, 4), (2, 6-7), (3, 9-10)$
9	532 ± 20	$([^2S_{1/2}]6p, [^2S_{1/2}]10p - 1[^2S_{1/2}]2p), ([^2S_{1/2}]9p, 1-2), ([^2S_{1/2}]10p, 2), ([^2S_{1/2}]11p, 3), ([^2S_{1/2}]12p, 3)$

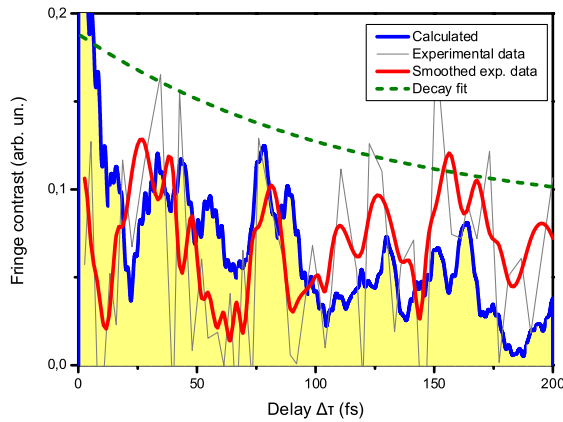


FIG. 4 (color online). Comparison of the calculated [blue (dark grey) line] and measured (thin grey line) fringe contrast of the autoionization signal. The thin grey line depicts the fringe contrast of the raw data of the recorded trace in Fig. 3(a). The moving average of the fringe contrast of the raw data is shown as a red (light grey) line. The green dashed line is an exponential decay fit on the raw data.

from the experimental data (thin grey line). The moving average of the fringe contrast of the raw data is shown as a red (light grey) line. In this figure, the calculated data have been multiplied by a constant in order to bring the calculated and measured data to approximately the same scale. This does not affect the positions of the maxima and minima. The calculated and experimental data appear to be in reasonable agreement. The dashed green line in Fig. 4 is an exponential [$y \propto \exp(-\Delta\tau/\tau_D)$] fitted to the maxima of the fringe contrast. The resulting $\tau_D = 140 \pm 90$ fs is a “weighted average” lifetime of the manifolds and is in good agreement with measured lifetime values.

In conclusion, we present time-resolved studies and Fourier transform spectroscopy utilizing extreme-ultraviolet radiation continua. The method allows the tracking of ultrafast electronic wave-packet dynamics exhibiting oscillatory and exponential decay evolution. The method is applied here to the superposition of a coherently excited autoionizing manifold, the decay of which facilitates detection, but can be applied to non-self-decaying states by absorption of a second photon leading to photoionization [21]. Total spectral widths that can be treated in one run may be extended to a few tens of eV or, equivalently, to a sub-100-as temporal resolution. On top of this, the energy resolution can be increased by simply increasing the total length of the delay line. This method, demonstrated here for the electronic motion of an atomic system,

can be applied to electronic or nonelectronic ultrafast dynamics of more complex systems in all states of matter.

This work is supported in part by the Ultraviolet Laser Facility (ULF) operating at FORTH-IESL (Contract No. HPRI-CT-2001-00139), the ELI research infrastructure preparatory phase program, the FASTQUAST ITN (Contract No. CA-ITN-214962), the ATTOFEL ITN, and the FLUX program (Contract No. PIAPP-GA-2008-218053) of the 7th FP.

*Corresponding author.

ptzallas@iesl.forth.gr

- [1] R. Loudon *The Quantum Theory of Light* (Oxford University, New York, 2000), pp. 102–103, 3rd ed.
- [2] N. F. Ramsey, *Phys. Rev.* **76**, 996 (1949); N. F. Ramsey, *Molecular Beams* (Oxford University, New York, London, 1956); M. M. Salour, *Rev. Mod. Phys.* **50**, 667 (1978); R. R. Jones *et al.*, *Phys. Rev. Lett.* **71**, 2575 (1993); M. B. Campbell, T. J. Bensity, and R. R. Jones, *Phys. Rev. A* **57**, 4616 (1998); M. Bellini, A. Bartoli, and T. W. Hansch, *Opt. Lett.* **22**, 540 (1997).
- [3] S. Cavalieri *et al.*, *Phys. Rev. Lett.* **89**, 133002 (2002).
- [4] F. Krausz and M. Ivanov, *Rev. Mod. Phys.* **81**, 163 (2009).
- [5] P. Tzallas *et al.*, *Nature Phys.* **3**, 846 (2007).
- [6] E. Skantzakis *et al.*, *Opt. Lett.* **34**, 1732 (2009).
- [7] E. Constant *et al.*, *J. Phys. IV (France)* **11**, Pr2-537 (2001).
- [8] P. Tzallas *et al.*, *Nature (London)* **426**, 267 (2003).
- [9] Y. Nabekawa *et al.*, *Phys. Rev. Lett.* **96**, 083901 (2006).
- [10] O. Faucher *et al.*, *Appl. Phys. B* **97**, 505 (2009).
- [11] S. Cavalieri and R. Eramo, *Phys. Rev. A* **58**, R4263 (1998); A. Pirri *et al.*, *Phys. Rev. A* **78**, 043410 (2008).
- [12] U. Fano and J. W. Cooper, *Rev. Mod. Phys.* **40**, 441 (1968); P. Lambropoulos and P. Zoller, *Phys. Rev. A* **24**, 379 (1981).
- [13] Yu. Ralchenko *et al.*, NIST Atomic Spectra Database (2008), <http://physics.nist.gov/asd3>.
- [14] K. Codling and R. P. Madden, *J. Res. Natl. Bur. Stand., Sect. A* **76**, 1 (1972).
- [15] D. L. Ederer, *Phys. Rev. A* **4**, 2263 (1971).
- [16] W. F. Chan *et al.*, *Phys. Rev. A* **46**, 149 (1992).
- [17] Z.-S. Yuan *et al.*, *J. Phys. B* **39**, 5097 (2006).
- [18] A. Kirrander and H. H. Fielding, *J. Phys. B* **40**, 897 (2007).
- [19] N. A. Papadogiannis *et al.*, *Phys. Rev. Lett.* **90**, 133902 (2003); D. Xenakis *et al.*, *J. Phys. B* **29**, L457 (1996).
- [20] A. V. Oppenheim and R. W. Schaffer, *Discrete-Time Signal Processing*, Prentice Hall Processing Series (Prentice-Hall, Upper Saddle River, NJ, 1999), 2nd ed.
- [21] A. Peralta Conde *et al.*, *Phys. Rev. A* **79**, 061405(R) (2009).